Proceedings of the 2020 International Manufacturing Science And Engineering Conferences
MSEC2020
June 22-June 26, 2020, Cincinnati, USA

MSEC2020-8454

SIMULTANEOUS MATERIAL MICROSTRUCTURE CLASSIFICATION AND DISCOVERY VIA HIDDEN MARKOV MODELING OF ACOUSTIC EMISSION SIGNALS

Xinyu Zhao
School of Computing, Informatics,
and Decision Systems Engineering
Arizona State University
Tempe, Arizona, 85281, USA

Ashif Iquebal
Department of Industrial
and Systems Engineering
Texas A&M University
College Station, Texas, 77840, USA

Huifeng Sun, Hao Yan*
School of Computing, Informatics,
and Decision Systems Engineering
Arizona State University
Tempe, Arizona, 85281, USA
Email*: haoyan@asu.edu

ABSTRACT

Acoustic emission (AE) signals have been widely employed for tracking material properties and structural characteristics. In this study, we aim to analyze the AE signals gathered during a scanning probe lithography process to classify the known microstructure types and discover unknown surface microstructures/anomalies. To achieve this, we developed a Hidden Markov Model to consider the temporal dependency of the high-resolution AE data. Furthermore, we compute the posterior classification probability and the negative likelihood score for microstructure classification and discovery. Subsequently, we present a diagnostic procedure to identify the dominant AE frequencies that allow us to track the microstructural characteristics. Finally, we apply the proposed approach to identify the surface microstructures of additively manufactured Ti-6Al-4V and show that it not only achieved a high classification accuracy (e.g., more than 90%) but also correctly identified the microstructural anomalies that may be subjected further investigation to discover new material phases/properties.

NOMENCLATURE

Λ The Hidden Markov Model
$\mathbf{Q}$ The set of hidden states of Hidden Markov Model
K Total number of hidden states
$S_{i,t}$ System state at time t for unit i
$\mathbf{A}$ The transition probability matrix of Hidden Markov Model
$p_{kk'}$ The transition probability that the system state is changed from k to k'
$O_{i,t}$ The observation at time t for unit i
O_{tj} The jth feature of observation at time t
T The length of observation sequence
$\mathbf{B}$ The emission matrix of Hidden Markov Model
μ_k The mean of multiple sensors in state k
σ_k The covariance matrix of multiple sensors in state k
$\mathbf{\Pi_i}$ THe initial state vector for unit i
$\pi_{i,k}$ The probability of initial state being k for unit i

INTRODUCTION

Throughout history, the process of discovering new materials has been slow, largely due to the combinatorial nature of identifying the "correct" material combination/composition as well as the time-consuming characterization tests (such as X-ray diffraction, electron microscopy) to ensure the quality and integrity of the materials. Recent breakthroughs in additive and hybrid manufacturing technologies have accelerated the fabrication of geometrically complex as well as functionally graded components [1, 2]. However, the process of characterizing the material properties and microstructure is still slow, creating a bottleneck in the discovery of novel materials [3, 4].

In recent years a major thrust has been towards developing novel approaches to enable rapid, in-situ characterization of material structure and property [5]. For instance, authors in [6] developed a novel approach to track the deformation mechanism while performing the tensile testing by recording the ultrasonic

vibrations. Such an approach allowed rapid materials characterization, potentially eliminating the need for costly experimentation such as X-ray diffraction. Along a similar direction, [7] utilized the capability of high-resolution acoustic emission sensing (with sampling rates exceeding 1000 kHz) and nanolithography together with machine learning to identify the microstructural fingerprint of Ti-6Al-4V. A nanolithography process essentially involves creating scratches on the surface of a given material via the controlled motion of a diamond indenter [8]. The methodology harnessed the capability of a nanoindenter to selectively probe the surface microstructures as the indenter scans through the surface. The corresponding AE response—originating from various physical transformation mechanisms such as plastic deformation, shear localization, etc.—captures the microstructural fingerprint of the material. More specifically, [7] showed that the AE spectrum in the range of 0.3-1 kHz and 30-50 kHz was able to distinguish different microstructure types in additively manufactured Ti-6Al-4V. AE sensing has been extensively employed in previous works. For instance, [9, 10] employed AE to study the strength of materials, [11] used AE to analyze the wear characteristics and [12, 13] studied the crack propagation using AE sensing.

This cheap deployment of the AE sensors with the nanolithography process offers a great possibility for fast mapping of the microstructures with relatively lower costs and efforts. However, AE sensors produce very high-resolution time-series data with complex temporal dependency, which requires advanced data science techniques to handle. Recently, a few works have focused on analyzing the AE data. For example, classification models were developed in [7, 14] to classify the microstructure types of the underlying material. However, despite the ability to classify known microstructures, these works failed to detect new or unknown types of materials.

The objective of this work is to assess how to utilize the AE sensor data to accurately discern the microstructure types by using AE sensing of a nanolithography process while simultaneously allowing the discovery of unknown materials microstructure. To achieve this goal, we present a hidden Markov model (HMM) approach, which is a generative classification model considering the temporal structure of the AE signal. We further develop techniques to classify the known material microstructures and detect new material microstructures simultaneously. Here, the detected new microstructure can either be a defect on the surfaces or new types of material produced by the manufacturing processes, which require further material characterization such as SEM or XRD.

In conclusion, the major contribution of the paper is 1) to build an HMM model for the AE signals considering the temporal consistency. 2) to classify known material microstructures using the posterior distribution of the material microstructure types given the AE signals. 3) to quantify how likely the region is "new material" by the negative likelihood score and provide a diagnostics tool on which feature is the leading factor for this behavior.

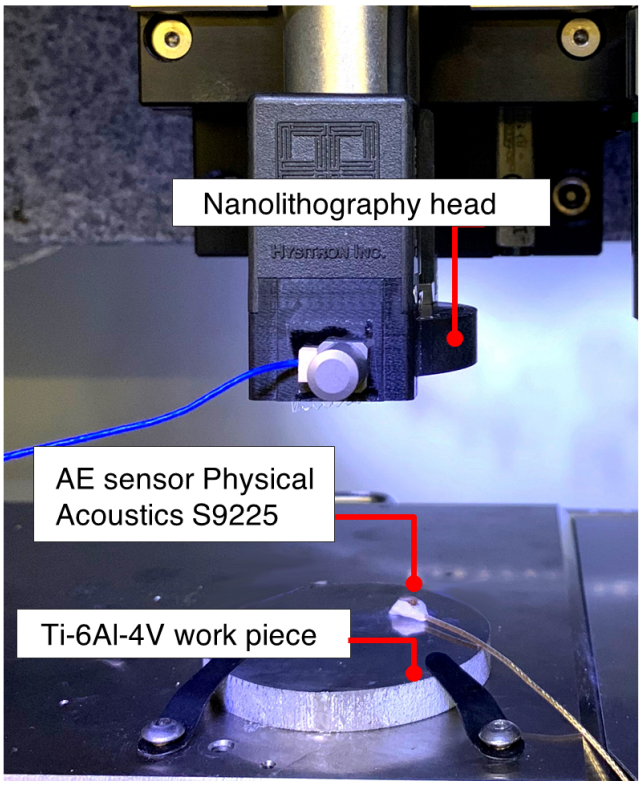

FIGURE 1: The Ti-6Al-4V workpiece sample is mounted inside the Hysitron TI 950 nanoindentation setup. The AE sensor was attached to the workpiece surface by using dental cement.

To validate the proposed methodology, we first present our experimental setup consisting of a nanoindentation setup to collect AE signals during the lithography process on the Ti-6Al-4V sample surface fabricated via additive manufacturing. Then, we will present the proposed modeling framework to discriminate different material microstructures as well as detecting if any particular region belongs to any known microstructure by the negative likelihood sore. Further diagnostics tools are proposed to understand which feature is the leading factor of such behavior. We will give a case study on how the proposed framework is used to discover a potential "new material region" in our real experiments. Finally, we will conclude the paper with the conclusions and future works.

EXPERIMENTAL DETAILS

Scanning probe lithography referred to as lithography in the rest of the manuscript employs a nanoindentation tool for texturing patterns on the surface of a given material. As a result of selectively probing the surface, the lithography process offers an approach to rapidly track the microstructural fingerprint of the

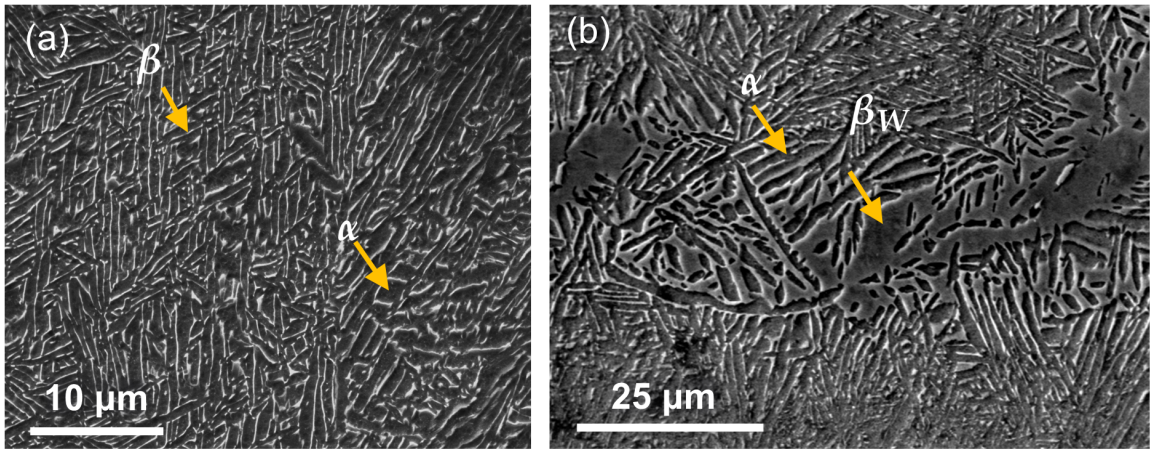

FIGURE 2: (a) A representative SEM image of the microstructure as observed in the as-fabricated workpiece. The microstructure comprises of $\alpha+\beta$ colony with α lamellar interspersed with rod-shaped β phase. (b) A representative microstructure obtained after the polishing was performed on the workpiece. The image shows evidence of extreme coarsening of the β phase at scattered locations. These are marked as β_W.

material under investigation [15] by recording the micro-elastic pulses generated as the indenter scans the surface. In this section, we present the description of sample fabrication and preparation, microstructure details, lithography experiments, and data collection.

Sample preparation

In the present work, we perform the lithography on Ti-6Al-4V workpiece samples fabricated using an electron beam melting (EBM) process. The as-fabricated workpiece was subsequently subjected to a multi-step finishing process on a hand-held Buehler Metaserv grinder-polisher (model 95-C2348-160). The finishing process employed Silicon Carbide (SiC) polishing pads with progressively reducing abrasive sizes (600 grits to 1200 grits). To impart a specular finish ($S_a \leq 25$ nm), the surface was finally polished using alumina abrasives of size 0.05 μm suspended in an aqueous solution with abrasive concentration at 20% by weight and pH ≈ 7.5. Throughout the polishing process, a nominal down pressure of 0.5kPa was maintained. The polisher was set to 500 revolutions per minute while ensuring a quasi-random motion. To observe the microstructures, the polished surface was etched with Kroll's reagent ($5-7$% nitric acid, $2-4$% hydrofluoric acid, and rest distilled water) for 10 seconds and rinsed thoroughly with distilled water. The microstructure was then observed under a scanning electron microscope (SEM) under high vacuum conditions.

Microstructure analysis

The polished surface comprised of standard α and β microstructures organized in colonies as well as basket-weave morphology. A representative SEM image of the microstructure is shown in Figure 2(a) with lamellar α phase in gray and the rod-shaped β phase in white. For modeling purposes, we refer to this $\alpha+\beta$ microstructure as the "standard microstructure". From a quantitative standpoint, the standard microstructure is primarily comprised of $\sim$90% α phase with $\sim$10% β phase.

A recent study has shown that mechanical polishing of as-fabricated Ti-6Al-4V workpiece under dry conditions result in the dilation of the β phase due to high temperatures (in the range of 700-1000 K) at the asperity-abrasive contacts during polishing [16]. We refer to this microstructure type, with widened β phase, as the diffused microstructure. This is labelled as β_W in Figure 2(b) and is composed of roughly 60% α and 40% β. Such non-equilibrium microstructures offer a unique potential to tailor the mechanical behavior of the workpiece such as the hardness and tensile strength of additively manufactured components for specific applications [17].

Lithography studies

In this work, lithography studies were performed on a sensor integrated nanoindentation setup consisting of a Hysitron TI 950 Triboindenter carrying a Berkovich indenter with a diamond tip with tip specification as: included angle – 142.3°, tool tip radius – 100 nm, and maximum allowable downforce - 10,000 μN. The effect of external disturbances is attenuated by installing a vibration isolating platform underneath. To perform lithography experiments, three locations on the surface were identified via SEM. Each of these three locations consisted of standard and diffused microstructure types. Five parallel scratches were created at each of the standard and diffused microstructure regions and

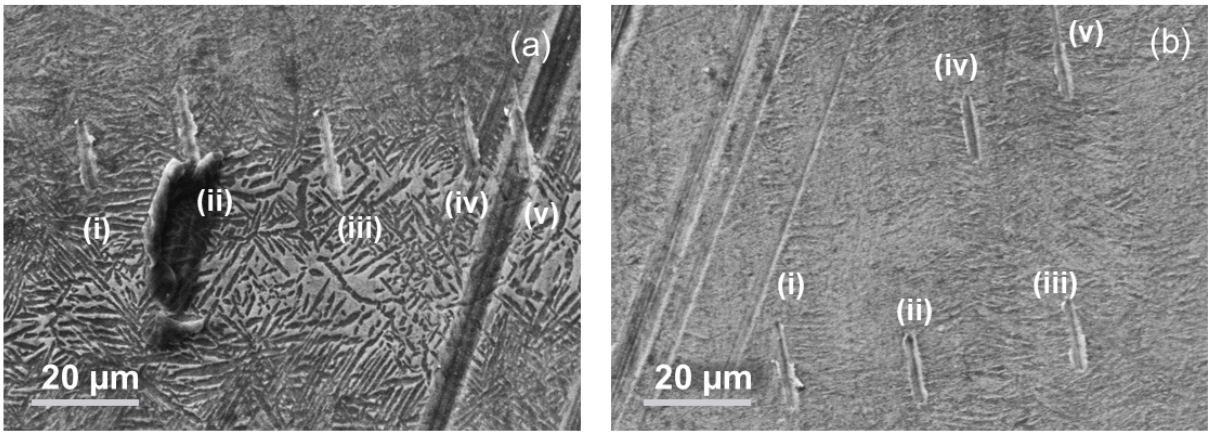

FIGURE 3: A representative SEM image of the (a) diffused and (b) standard microstructure regions showing the five distinct scratches generated during the lithography process.

representative SEM images are shown in Figures 3(c & d). The scratches are marked as (i), (ii), (iii), (iv), and (v) and are each of length 15 μm. The length of the scratch was selected to 15 μm to ensure that most of the primary microstructural features were scanned by each of the scratches such as the widths of the rod-shaped β and the diffused β_W phases. The indenter speed was set to 0.5 μm/sec, such that each scratch lasted for 30 sec. The AE released during the process was collected using a S9225 AE sensor from Physical Acoustic Corp with a sampling frequency of 300-1800 kHz. The aforementioned lithography process was repeated at three random locations, each containing predetermined diffused and standard microstructures, as depicted in Figure 3(a).

Proposed Modeling Frameworks

In this work, we propose a framework to classify the known underlying microstructure of the material and identifying defects or unknown microstructure based on signals from AE sensors. To achieve this, we build a hidden Markov model (HMM) as a temporal generative model to achieve both goals. We will first give a brief introduction of the HMM model and then discuss how to use this model for both known microstructure classification and unknown microstructure detection.

Hidden Markov Model

HMM is a probabilistic model that describes the transitions of a finite number of states over time. These states characterize two stochastic processes: the hidden state transition in the discrete-time and observed process. In addition, three sets of probability distributions are utilized to characterize the system dynamics: the initial probabilities for all the hidden states; the transition probabilities between two hidden states, and the emission probabilities of an observation from a hidden state. The elements of an HMM are defined as follows:

1) Let $\mathbf{Q} = \{1, \cdots K\}$ denote the set of hidden states, with the total number of states to be K. We denote $S_{i,t} \in \mathbf{Q}$ as the system state at time t for unit $i \in \{1, \cdots, n\}$. Furthermore, we denote $S_{i,t}^k$ as a binary variable according to whether the system for unit i at state k in time t.

2) A transition probability matrix is defined as $\mathbf{A} = \{p_{kk'}\}$, in which $p_{kk'}$ is the transition probability that the system state is changed from state k to state k', $k, k' \in \{1, \ldots, K\}$ at time t,

$$p_{kk'} = P(S_{i,t+1} = k | S_{i,t} = k'), 1 \leq k, k' \leq K. \tag{1}$$

An emission probability is defined on multi-variate response $\mathbf{O}_{i,t}$ by two sets of matrix $\mathbf{B} = \{\boldsymbol{\mu}_k, \boldsymbol{\Sigma}_k\}$, in which $\boldsymbol{\mu}_k$ is the mean of multiple sensors in state k, and $\boldsymbol{\Sigma}_k$ denote the covariance matrix of multiple sensing measurement. In other words,

$$\begin{aligned}(\mathbf{O}_{i,t} | S_{i,t} = k) \sim & N(\boldsymbol{\mu}_k, \boldsymbol{\Sigma}_k), \\ & i = 1, \cdots, n, k = 1, \cdots, K.\end{aligned} \tag{2}$$

An initial state vector $\boldsymbol{\Pi}_{\boldsymbol{i}} = \{\pi_{i,k}\}$ is defined to express the distribution of the system states for unit i at state k at $t = 1$.

With the descriptions shown above, for the simplicity and clarification, the full HMM model is given by $\Lambda = \{\mathbf{Q}, \mathbf{A}, \mathbf{B}, \boldsymbol{\Pi}_{\boldsymbol{i}}\}$. Figure 4 shows the logical dependencies among different random variables of an HMM. Furthermore, three major problems can be solved by the HMM [18]:

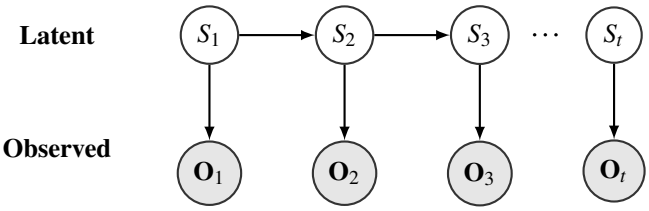

FIGURE 4: Illustrative picture of HMM, the S_i's are the hidden or latent state variable and $\mathbf{O}_i$'s are the observed variables

1) *Evaluation problem*- Given an HMM Λ and an observation sequence $\{\mathbf{O}_{i,t}\}_{t=1}^{T} = (\mathbf{O}_{i,1}, \mathbf{O}_{i,2}, \ldots, \mathbf{O}_{i,T})$, find the probability that the sequence $\{\mathbf{O}_{i,t}\}_{t=1}^{T}$ is accrued, or $P(\{\mathbf{O}_{i,t}\}_{t=1}^{T}|\Lambda)$, using the HMM modeling. The evaluation problem an be used to evaluate both the sequence likelihood $P(\{\mathbf{O}_{i,t}\}_{t=1}^{T}|\Lambda)$ and the individual point likelihood $P(\{\mathbf{O}_{i,t}\}|\Lambda)$

2) *Decoding problem*- Given an HMM Λ and an observation sequence $\{\mathbf{O}_{i,t}\}_{t=1}^{T}$, identify the system state at each time t or estimate $P(S_{i,t}|\{\mathbf{O}_{i,t}\}_{t=1}^{T})$. The decoding problem will be related to the microstructure identification process.

3) *Learning problem*- Find the parameters in the model Λ (the $\mathbf{A}, \mathbf{B}, \mathbf{\Pi_i}$) that maximize the probability $P(\{\mathbf{O}_{i,t}\}_{t=1}^{T}|\mathbf{A}, \mathbf{B}, \mathbf{\Pi_i})$.

For more details of using the Expectation-Maximization algorithms and the forward-backward algorithms to solve these three problems, please refer to [18]. We will then review how to use the three problems to solve the problems of microstructure classification and new material discovery. First, the parameters of the HMM models need to be learned by solving the learning problem. Then we propose to use the decoding problem and evaluation problem to solve the problem of microstructure classification and material discovery.

Microstructure Classification

We propose to differentiate known underlying material microstructures by solving the decoding problem in HMM. With model parameters determined, we are able to classify the observation by solving a decoding problem to find the probability $P(S_t = k|\{O_t\}_{t=1}^{T})$. The decoding problem is used solved through the Forward-backward algorithm by decomposing the equation into two terms $P(O_1, \ldots, O_t, S_t = k, O_{t+1})$ and $P(O_{t+1}, \ldots, O_T|S_t = k)$, and solve both terms using the dynamic programming. Here, we will classify the microstructure according to the largest posterior distribution $\hat{k}_t = \arg\max_k P(S_t = k|\{O_t\}_{t=1}^{T})$

Material Discovery

Given the trained HMM Λ, we denote the sequence with low likelihood $P(O_1, O_2, \ldots, O_t|\Lambda)$ as the sequence with potential new material. We can also calculate the likelihood for a single point $P(\{\mathbf{O}_{i,t}\}|\Lambda)$ by summing up all possible states $\sum_{j=1}^{K} P(O_t|S_t = j)$. In this way, the problem of material discovery can be solved by the evaluation problem in HMM.

Diagnostics for Material Discovery

We further analyze which feature is the leading factor that the HMM quantifies the sequence as the "new material" sequence. To achieve this, we find that under the assumption that the covariance matrix of the emission is a diagonal matrix, the likelihood score can be decoupled into the likelihood of each individual feature. For example, if we know that all features O_{tj} of observation at time t are independent, the log-likelihood can be decoupled as following:

$$\log P(O_t|\Lambda) = \sum_j \log P(O_{tj}|\Lambda) \tag{3}$$

O_{tj} represents the jth feature of observation O_t. With this decoupled likelihood, we are able to calculate the likelihood of each feature seperately.

Case Study

Finally, we will apply the proposed methodology to the real case study. The acoustic emission (AE) signals are collected from a nanolithography process, described in the experimental setup. We have collected five parallel scratches from the three locations. For each scratch, it is divided into segments with 0.25s. with 125000 ($= 0.25 \times 500,000$) data points. Each of these segments is labeled as either diffused and standard microstructure. Therefore, we have in total 600 ($= 30\text{sec} \times (1/0.25\text{sec}) \times 5.$) samples from each class of microstructure.

We further preprocess the AE sensor signal in the following data processing pipeline:

1) Each time slice was transferred into the Fourier domain with 62500 data points for each set. As the sampling rate of the AE data was 500 kHz, the frequency range of 0-250 kHz could only be observed.
2) The entire frequency band is further divided into 50 non-overlapping intervals (each representing a frequency range of 5 kHz.
3) The root mean square values of the power in each of these intervals are calculated as features.

After the preprocessing, the dataset comprises 600 sample observations and 50 features for each class (Standard/ Diffused) on each location. Fig. 5 shows several selected frequency bands

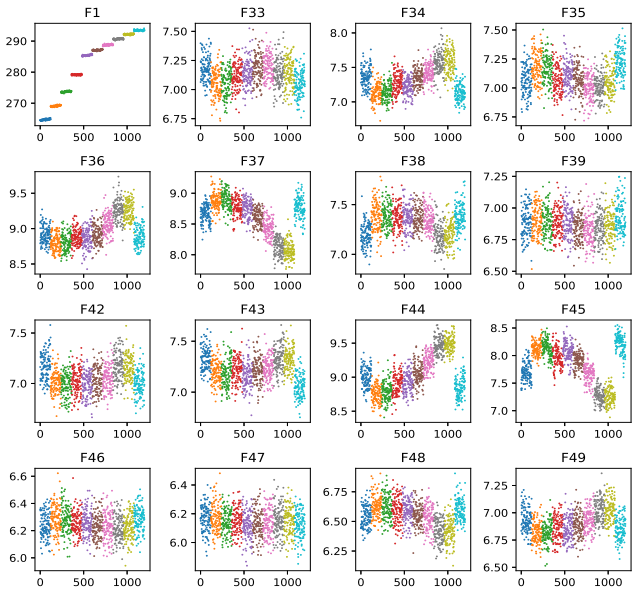

FIGURE 5: AE sensor signal from frequency domain. Ten different colors represent the diffused microstructures and standard microstructures from left to right.

(e.g. F1, F33-F50) of AE sensor signal. The different color shows the samples from different scratches. The first five scratches are diffused phase, and the last five are standard phases.

From Fig. 5, it seems that F1 is very sample-dependent since all ten scratches share very different F1 features. Furthermore, standard V (e.g., shown in the light blue color) has very different F44 and F45 values.

For the microstructure classification, Fig. 6a shows the classification results from HMM. From the results, we can see that we are able to classify most of the sequences except Diffused V. We further calculate the likelihood of each sequence and present the results as Fig. 6b. We can find that Diffused V got the wrong prediction, which is due to that this Diffused V gets a very low likelihood score compared to others. In order to understand the reason for it, we did a diagnostic process by decomposing the likelihood score of a sequence into the likelihood score of the features of the sequence. To report the accuracy, we can conclude that all standard structures are predicted correctly and diffused structures are predicted correctly except diffused V.

Fig. 6b shows the sequence of negative likelihood among ten observed locations. From this figure, we see that diffused V, standard IV, and standard V locations will have a lower likelihood than other locations. Among these, diffused V has the lowest likelihood score. The lower likelihood score shows that the model is not very confident in modeling these scratches, partially due to that these scratches are different from others.

Both Fig. 7a and Fig. 7b are identified as the “new material”,

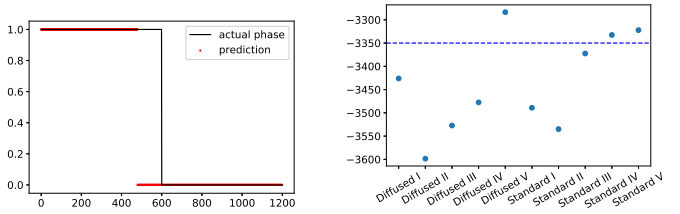

(a) Prediction Accuracy

(b) Negative Likelihood Score of Each Sample

FIGURE 6: Results of Material Microstructure Classification and Material Discovery. (a) shows the prediction accuracy compared the prediction labels (shown in red) with the true labels (shown in black). (b) shows the negative likelihood score to identify each sample being new material/anomaly.

the likelihood score of diffused phase is much smaller than that of the standard phase of feature ‘F1’, so feature ‘F1’ is a quite important factor which influences the prediction results. These two plots are consistent with the results showed from the sequence likelihood in Fig. 6b. Furthermore, the overall likelihood score for diffused and standard are smaller, which contributes to the decision of ”new material”. For Diffused V, this finding is consistent with the SEM images reported as shown in Fig. 8a, where Diffused V seems to be in a slightly darker region and the ‘F1’ frequency is much closer to the standard material. For Standard V, ‘F45’ shows as the second important feature contributing to the low overall likelihood score. This can be seen from Fig. 8b, where both ‘F43’ and ‘F45’ have very different frequency features from the rest and SEM images show a slightly darker region on the Standard V. For Diffused IV and Standard II are both detected as the “normal material” and classified correctly. Interesting, we can see that despite that ‘F1’ is still the leading factor for the classification. F32-F45 are also important factors that contribute to the classification and material discovery decision. These findings are in alignment with the findings in [7].

CONCLUSION

In this work, we analyzed the acoustic emission signals generated from a lithography process for material microstructure classification and new materials discovery. In order to achieve these two objectives we propose a pipeline to extract the important frequency features from the raw signals and model the sequential data with Hidden Markov Model. We also discussed three possible applications of Hidden Markov Model. Firstly, we are able to differentiate different microstructure by solving an evaluation problem in HMM. Our results show that we can capture all sequences except one sequence. We further discover that this sequence is potentially a new material microstructure/phase due to the low likelihood score. We further confirmed this finding

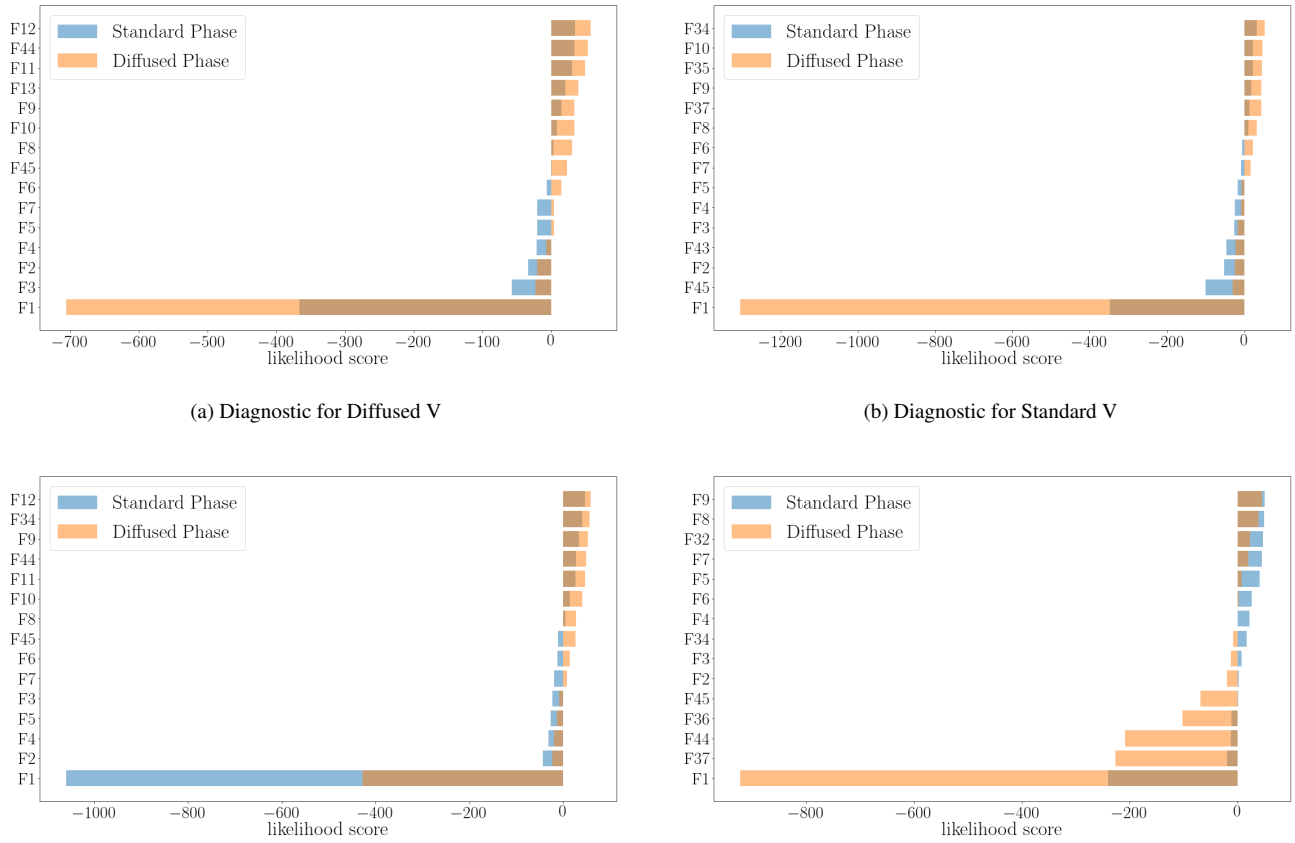

(a) Diagnostic for Diffused V

(b) Diagnostic for Standard V

(c) Diagnostic for Diffused IV

(d) Diagnostic for Standard II

FIGURE 7: (a) and (b) are the scratches that have been identified as "new material". (c) and (d) are identified as normal samples. As can be seen from all figures, F1 is always associated the low-likelihood score due to the large sample-to-sample variations.

with the SEM images. Finally, we conduct a diagnosis process on all sequences by decomposing the log-likelihood of HMM. Through the process, we find that the root cause of diffused V being identified as the new material is due to the F1 feature.

While the proposed method is not supposed to replace the traditional high-fidelity measurements such SEM or XRD, it offers an approach to rapid gather low-fidelity information about the material microstructure that can be used as a guide to search for novel materials, therefore, significantly reducing the experimental efforts. In the future work, we will study how to combine both AE signals (low-fidelity) and SEM images or XRD (high-fidelity) for efficient material discovery.

REFERENCES

[1] Chen, L.-Q., Chen, L.-D., Kalinin, S. V., Klimeck, G., Kumar, S. K., Neugebauer, J., and Terasaki, I., 2015. "Design and discovery of materials guided by theory and computation". *npj Comput Mater,* ***1***, p. 15007.

[2] Sames, W. J., List, F., Pannala, S., Dehoff, R. R., and Babu, S. S., 2016. "The metallurgy and processing science of metal additive manufacturing". *Int Mat Rev,* ***61***, pp. 315–360.

[3] Aspuru-Guzik, A., and Persson, K., 2018. Materials acceleration platform: Accelerating advanced energy materials discovery by integrating high-throughput methods and artificial intelligence. Tech. rep.

[4] Alberi, K., Nardelli, M. B., Zakutayev, A., Mitas, L., Curtarolo, S., Jain, A., Fornari, M., Marzari, N., Takeuchi, I., Green, M. L., et al., 2018. "The 2019 materials by design roadmap". *J Phys D Appl Phy,* ***52***, p. 013001.

[5] de Pablo, J. J., Jones, B., Kovacs, C. L., Ozolins, V., and Ramirez, A. P., 2014. "The materials genome initiative, the interplay of experiment, theory and computation". *Current Opinion in Solid State and Materials Science,* ***18***(2), pp. 99–117.

[6] Min, X.-H., Kato, H., Narisawa, N., and Kageyama, K.,

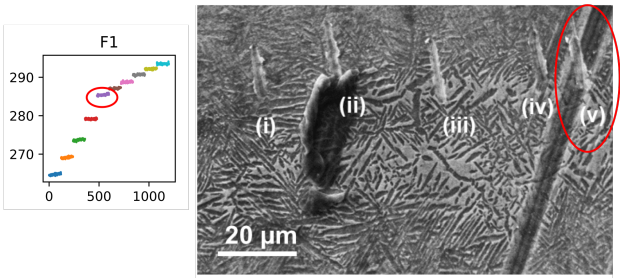

(a) Diffused V

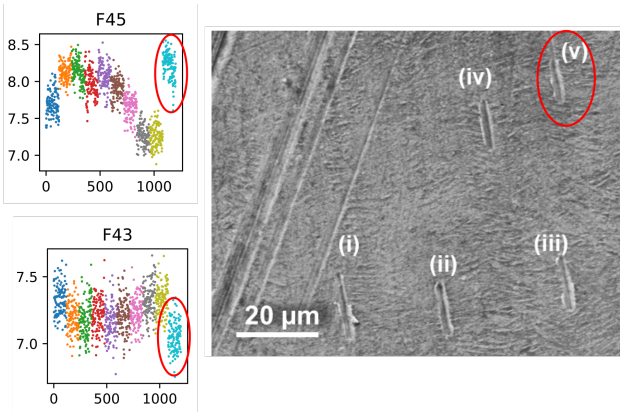

(b) Standard V

FIGURE 8: Diagnostics plot for Diffused V and Standard V

2005. "Real-time ultrasonic measurement during tensile testing of aluminum alloys". *Materials Science and Engineering: A,* ***392***(1-2), pp. 87–93.

[7] Iquebal, A. S., Pandagare, S., and Bukkapatnam, S., 2019. "Learning acoustic emission signatures from a nanoindentation-based lithography process: Towards rapid microstructure characterization". *Tribology International*, p. 106074.

[8] Botcha, B., Wang, Z., Rajan, S., Gautam, N., Bukkapatnam, S. T., Manthanwar, A., Scott, M., Schneider, D., and Korambath, P., 2018. "Implementing the transformation of discrete part manufacturing systems into smart manufacturing platforms". In ASME 2018 13th Int Manuf Sci Eng Conf, ASME, pp. V003T02A009–V003T02A009.

[9] De Bono, D. M., London, T., Baker, M., and Whiting, M. J., 2017. "A robust inverse analysis method to estimate the local tensile properties of heterogeneous materials from nano-indentation data". *Inte J Mech Sci,* ***123***, pp. 162–176.

[10] Karimi, N. Z., Heidary, H., and Ahmadi, M., 2012. "Residual tensile strength monitoring of drilled composite materials by acoustic emission". *Mat Des,* ***40***, pp. 229–236.

[11] Baccar, D., and Söffker, D., 2015. "Wear detection by means of wavelet-based acoustic emission analysis". *Mech Sys Signal Proc,* ***60***, pp. 198–207.

[12] Wisner, B., Mazur, K., Perumal, V., Baxevanakis, K. P., An, L., Feng, G., and Kontsos, A., 2019. "Acoustic emission signal processing framework to identify fracture in aluminum alloys". *Eng Fract Mech,* ***210***, pp. 367–380.

[13] Sause, M., Müller, T., Horoschenkoff, A., and Horn, S., 2012. "Quantification of failure mechanisms in mode-I loading of fiber reinforced plastics utilizing acoustic emission analysis". *Comp Sci Tech,* ***72***, pp. 167–174.

[14] Wei, Q., Lü, J., Yang, Q., and Li, X., 2018. "Multi-pass micro-scratching and tribological behaviors of an austenitic steel in media". *Trib Int,* ***117***, pp. 112–118.

[15] Chang, D.-C., and Bukkapatnam, S., 2004. "Towards characterizing the microdynamics of ae generation in machining". *Mach Sci Tech,* ***8***, pp. 235–261.

[16] Iquebal, A. S., Sagapuram, D., and Bukkapatnam, S. T., 2019. "Surface plastic flow in polishing of rough surfaces". *Sci Rep,* ***9***, p. 10617.

[17] Wang, Z., Palmer, T. A., and Beese, A. M., 2016. "Effect of processing parameters on microstructure and tensile properties of austenitic stainless steel 304L made by directed energy deposition additive manufacturing". *Acta Mater,* ***110***, pp. 226–235.

[18] Rabiner, L. R., 1989. "A tutorial on hidden markov models and selected applications in speech recognition". *Proceedings of the IEEE,* ***77***(2), pp. 257–286.